REPUBLIQUE ALGERIENNE DEMOCRATIQUE ET POPULAIRE

MINISTERE DE L'ENSEIGNEMENT SUPERIEUR ET DE LA RECHERCHE SCIENTIFIQUE

UNIVERSITE SAAD DAHLAB DE BLIDA 1

FACULTE DE TECHNOLOGIE

DEPARTEMENT DE MECANIQUE

Projet de Fin d'Etudes

Pour l'obtention du Diplôme de Master en

Construction mécanique

Titre

Numerical simulation of the FIC by the ANSYS code of the semi-elliptical cracks which can develop in the pressure vessels

Encadré Par :
Mr. Madani fateh

Co-promoteur :
Dr. Djillali SAAD

Réalisé par :
SAAD Ayoub Abdelkhalek
Bouabdellah hamza

Année universitaire 2021/2022

Acknowledgements

First of all, I thank Almighty God for giving me the strength, courage and patience to accomplish this work.

I sincerely thank Mr. Fateh Madani for the help he gave me,

I extend my sincere thanks to the members of my family for their understanding, their encouragement and their help throughout the preparation of this letter, in particular my dear parents for the attention and moral support they have given me.

And all teachers and colleagues of Saad Dalb University, Department of Mechanical Engineering

ملخص

تعتبر الشقوق الطولية التي يمكن أن تتطور في أنابيب الضغط من المخاطر الخطيرة. تولد هذه التشققات بشكل عام في حالات انقطاع الهيكل مثل مفصل اللحام . من خلال هذه الدراسة ، تم اقتراح نموذج رقمي ثلاثي الأبعاد ، باستخدام برنامج ANSYS لحساب عامل شدة الإجهاد SIF .، على طول طرف الشق شبه الإهليلجي الطولي الموجود في جدار وعاء الضغط

Summary

Longitudinal cracks that can develop in pressure vessels are a critical hazard. These cracks are generally born in the discontinuities of the structure such as the weld joint. Through this study, a three-dimensional numerical model, using ANSYS software, is proposed for the calculation of the stress intensity factor (SIF) along the longitudinal semi-elliptical crack tip located in the wall of a pressure vessel.

Contents

Figures list

Tables list

General introduction

All mechanical parts contain cracks, even if it cannot be seen with the naked eye. These cracks can grow slowly or suddenly, the latter case often being synonymous with rupture; forecasting these phenomena is therefore an essential dimensioning issue. Rupture is a problem that man will have to deal with as long as he makes structures. This problem is increasingly crucial with the development, linked to technological progress, of complex structures.

In the design of pressure vessel, the use of fracture mechanics theory and non-destructive testing are the most effective tools for design engineers. Fracture mechanics is generally used to predict the failure of components caused by the preexistence of small cracks. It also allows us to take our precautions to stop any future propagation of the crack or to determine the life of the structure in the event that propagation is unavoidable.

In the case of an elastic material (brittle failure), one of the most used cracking criteria is the stress intensity factor (SIF). However, and because it is difficult to accurately determine the SIF for cracks in complex structures by analytical solutions, the use of numerical methods such as finite elements becomes the only appropriate tool.

We propose through this work, to study the toughness of pressure vessels widely used in industry. We will be particularly interested in the investigation of the effect of the ratio of the depth of the crack on the vessel thickness (a/t) and the effect of the ratio of the geometry of the crack (a/c) on the SIF.

The document is organized as follows:

A general introduction;

The first chapter gathers the elements of bibliography necessary for this study;

The second chapter is devoted to the validation of the numerical model produced by the ASME standard;

The last chapter deals with the numerical model developed as well as the discussion of the results;

The document ends with a general conclusion.

Chapter I: Bibliography

1.1 Introduction

Fracture is a problem that society has faced for as long as there have been man-made structures. This problem is increasingly crucial with the development, linked to technological progress, of complex structures.

The problem may actually be worse today than in previous centuries, because more can go wrong in our complex technological society.

However, many failure mechanisms are still poorly understood, in particular when using new materials or new processes. The cost of breakups catastrophic events represents,

according to economic studies carried out since the beginning of the 1980s, almost 4% of GNP in developed industrial countries. We can reduce this cost of about 30% by correctly applying the known concepts of the mechanics of rupture and an additional 25% by further developing research in the field of rupture.

1.3 Why Structures Fail

The cause of most structural failures generally falls into one of the following categories: Negligence during design, construction, or operation of the structure. Application of a new design or material, which produces an unexpected (and undesirable) result. In the first instance, existing procedures are sufficient to avoid failure, but are not followed by one or more of the parties involved, due to human error, ignorance, or willful misconduct. Poor workmanship, inappropriate or substandard materials, errors in stress analysis, and operator error are examples of where the appropriate technology and experience are available, but not applied.

The second type of failure is much more difficult to prevent. When an ‘‘improved” design is introduced, invariably, there are factors that the designer does not anticipate. New materials can offer tremendous advantages, but also potential problems. Consequently, a new design or material should be placed into service only after extensive testing and analysis. Such an approach will reduce the frequency of failures, but not eliminate them entirely; there may be important factors that are overlooked during testing and analysis.

One of the most famous Type 2 failures is the brittle fracture of World War II Liberty ships. These ships, which were the first to have all-welded hulls, could be fabricated much faster and cheaper than earlier riveted designs, but a significant number of these vessels sustained serious fractures as a result of the design change. Today, virtually all steel ships are welded, but sufficient knowledge was gained from the Liberty ship failures to avoid similar problems in present structures.

Knowledge must be applied in order to be useful, however, Figure. 1.1 shows an example of a Type 1 failure, where poor workmanship in a seemingly inconsequential structural detail caused a more recent fracture in a welded ship. On 15 March 1979, the Kurdistan oil tanker broke completely in two while sailing in the North Atlantic[2]. The combination of warm oil in the tanker with cold water in contact with the outer hull produced substantial thermal stresses. The fracture initiated from a bilge keel that was improperly welded. The weld failed to penetrate the structural detail, resulting in a severe stress concentration. Although the hull steel had adequate toughness to prevent fracture initiation, it failed to stop the propagating crack.

1.4 Fracture mechanics

Fracture mechanics has as its essential object the study of macroscopic cracks: it applies when there are discontinuities in the material, such in the material that they come to modify the state of stress, deformation and displacement, so that the homogenization of the medium no longer makes sense. The separation into two disjointed parts of a body occurs following the initiation phase, which saw the development of microcavities, micro fissures under the action of mechanical, thermal, chemical stresses The propagation of the macroscopic cracks can lead to the complete separation of several pieces or on the contrary the cracks can stop. The failure mode can be brittle, with failure often occurring without plastic deformation, in the presence of significant plastic deformation [3].

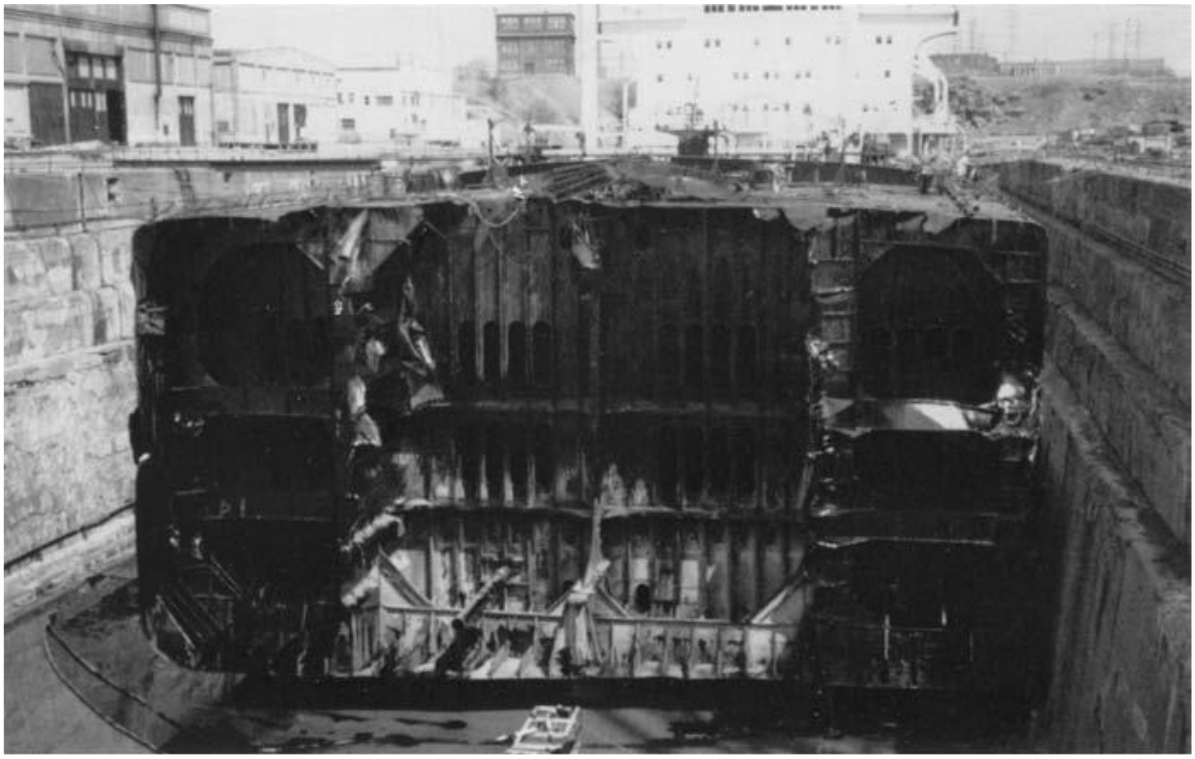

Figure 1.1 (a)

Figure 1.1 (b)

Figure 1.1: The MSV Kurdistan oil tanker, which sustained a brittle fracture while sailing in the North Atlantic in 1979: (a) fractured vessel in dry dock and (b) bilge keel from which the fracture initiated. (Photographs provided by S.J. Garwood.).

1.5 Failure Types

There are more than twenty different recognizable ways a material can fail, including the most common forms: fracture, fatigue, wear, and corrosion.[4]. Each of these and other common failure modes are described briefly in the following sections.

1.6 Brittle Fracture

Brittle fracture occurs when mechanical loads exceed a material's ultimate tensile strength causing it to fracture into two or more parts without undergoing any significant plastic deformation or strain failure. Material characteristics and defects such as notches, voids, inclusions, cracks, and residual stresses are the typical initiation points for the formation of a crack leading to brittle fracture (Figure. 1.2). Once the crack is initiated the material will undergo catastrophic failure fairly quickly under a sustained load. There is little energy absorbed (compared to ductile fracture) during the brittle fracture process. This failure mode commonly occurs in brittle materials such as ceramics and hard metals.

Eliminating or minimizing surface and internal material defects is an important method in improving a material's resistance to brittle fracture. Many of these defects originate during material fabrication or processing steps. Therefore, it is important to give these early stages in the life cycle proper attention in order to reduce the material's susceptibility to brittle fracture. Fabricating a part with a smooth surface is also important in preventing brittle fracture. For instance, sharp textures and notches on the surface of the material can initiate brittle fracture. Careful handling of the material after it's produced will also help to prevent unnecessary mechanical damage such as scratches and gouges, which can ultimately lead to brittle fracture. Finally, an appropriate materials selection process to choose a suitable material for the intended application is important in ensuring that it will be capable of handling the applied mechanical loads.

Figure 1.2: Brittle Fracture Surface of a High-Strength Chain. Fracture Began in a Small Crack Resulting from a Heat-Treating Problem (Photo Courtesy of Sachs, Salvaterra & Associates, Inc.).

1.7 Ductile Failure

Ductile materials that are subjected to a tensile or shear stress will elastically or plastically strain to accommodate the load and absorb the energy. Yielding occurs when the material's yield strength is exceeded and can no longer return to its original shape and size. This is followed by

ductile fracture which occurs when the deformation processes can no longer sustain the applied load. Both of these failure modes are illustrated in Figure. 1.3.

Figure 1.3: (a) Ductile Fracture of 2 1/2 Inch Hose Fitting (b) Close-up of the Deformed Region Where a Pin Joining the "Ears" Became Free from the One on the Right Causing the Deformation and Fracture of the One on the Left (Photos Courtesy of Sachs, Salvaterra & Associates, Inc.)

1.8 Thermal Relaxation

Thermal relaxation is a process related to the temperature dependent creep failure mode. Failure by thermal relaxation commonly occurs in fastener materials or other materials that are prestressed such that they could support a greater load than their non-prestressed counterpart. As the material undergoes creep at high temperatures their residual stresses are relieved which may render the material unable to support the given load.

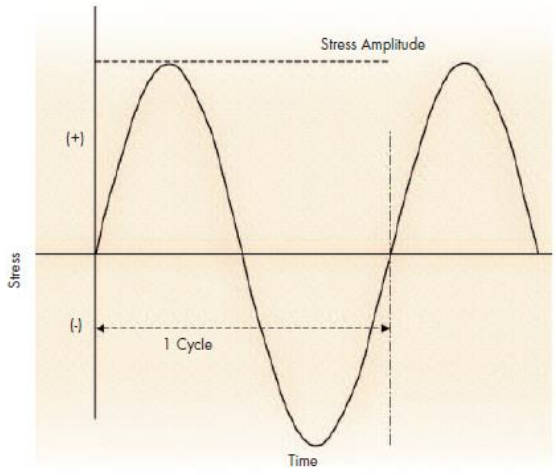

Figure 1.4: Fatigue Loading Cycle.

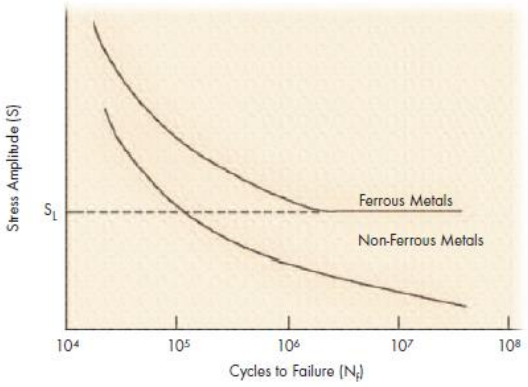

Figure 1.5: S/N Curves for Ferrous and Non-Ferrous Metals [1].

1.9 Fatigue

Fatigue is an extremely common failure mode and deserves considerable attention because it can inflict damage on a material at a stress level that is far less than the material's design limit. Fatigue has been attributed with playing a role in approximately 90% of all material structural failures[5].

A material that fractures into two or more pieces after being subjected to a cyclic stress (fluctuating load) over a period of time is considered to have failed by fatigue. The maximum value of the cyclic stress (stress amplitude) for fatigue failure is less than the material's ultimate tensile strength. It is often the case that the maximum value of the cyclic stress is so low that if it were applied at a constant level the material would be able to easily support the load without incurring any damage. Cyclic loads cause the initiation and growth of a crack, and ultimately, when the crack is significant enough such that the material can no longer support the load, the material fractures. The fatigue failure mechanism involves three stages: crack initiation, crack propagation, and material rupture.

Similar to both ductile and brittle fracture, fatigue cracks are often initiated by material inhomogeneities, such as notches, grooves, surface discontinuities, flaws, and other material defects[6].

These inhomogeneities or initiation points act as stress raisers where the applied stress concentrates until it exceeds the local strength of the material and produces a crack. The best way to prevent fatigue failure is to keep fatigue cracks from initiating, which can be accomplished by removing or minimizing crack initiators, or by minimizing the stress

amplitude. Once fatigue cracks have been initiated, they will seek out the easiest or weakest path to

propagate through the material. Therefore, minimizing the number of internal material defects, such as voids and inclusions, will increase the time it takes a crack to propagate. Finally, when the crack has weakened the material to a point such that it can no longer support the applied load it will rupture, which can occur by shear or by tension [7].

Fatigue is not so much dependent on time as it is the number of cycles. A cycle consists of an applied stress being increased from a starting value (in some cases, zero or even negative) up to a maximum positive value (material loaded in positive direction) and then decreasing past the starting point down to a minimum value (in some cases this is a maximum negative loading), and finally back up to the starting value. This cycle is illustrated in Figure. 1.4, where there is positive and negative loading. However, negative loading is not required for fatigue to occur; rather, it can be a fluctuating positive load. Moreover, the stress cycles do not need to be symmetric, but can be randomly changing. In general, ferrous, or iron alloy, materials do have a fatigue (endurance) limit (SL), which is the stress level (amplitude) under which no failure will occur regardless of the number of cycles. On the other hand, by increasing the stress amplitude, the fatigue failure will commence after a smaller number of cycles. Non-ferrous alloys, such as aluminum and titanium, do not have a fatigue limit because it will eventually fail even from small stresses. So, airplanes and bicycles use aluminum alloys and are overdesigned to prevent failure due to repeated stress. This concept is demonstrated in Figure. 1.4.

Metals and polymers are typically susceptible to fatigue failure, while ceramics tend to be resistant. There are several different types of fatigue including high-cycle fatigue, low-cycle fatigue, thermal fatigue, surface fatigue, impact fatigue, corrosion fatigue, and fretting fatigue.

1.10 Failure prevention

In general, the most effective ways to prevent a material from failing is proper and accurate design, routine and appropriate maintenance, and frequent inspection of the material for defects and abnormalities.

Proper design of a system should include a thorough materials selection process in order to eliminate materials that could potentially be incompatible with the operating environment and to select the material that is most appropriate for the operating and peak conditions of the system. If a material is selected based only on its ability to meet mechanical property requirements, for instance, it may fail due to incompatibility with the operating environment.

Therefore, all performance requirements, operating conditions, and potential failure modes must be considered when selecting an appropriate material for the system. Routine maintenance will lessen the possibility of a material failure due to extreme operating environments. For example, a material that is susceptible to corrosion in a marine environment could be sustained longer if the salt is periodically washed off. It is generally a good idea to develop a maintenance plan before the system is in service. Finally, routine inspections can sometimes help identify if a material is at the beginning stages of failure. If inspections are performed in a routine fashion, then it is more likely to prevent a component from failing while the system is in-service.

1.11 Stress analysis of cracks

For certain cracked configurations subjected to external forces, it is possible to derive closed-form expressions for the stresses in the body, assuming isotropic linear elastic material behavior. Westergaard [8], Irwin [9], Sneddon [10], and Williams [11] were among the first to publish such solutions. If we define a polar coordinate axis with the origin at the crack tip (Figure. 1.6), it can be shown that the stress field in any linear elastic cracked body is given by

$$\sigma_{ij} = \left(\frac{k}{\sqrt{r}}\right) f_{ij}(\theta) + \sum_{m=0}^{\infty} A_m r^{\frac{m}{2}} g_{ij}^{(m)}(\theta) \qquad (1.1)$$

Where,

σ_{ij}, stress tensor

r and θ are as defined in Figure. 1.6

k = constant

f_{ij}, dimensionless function of θ in the leading term

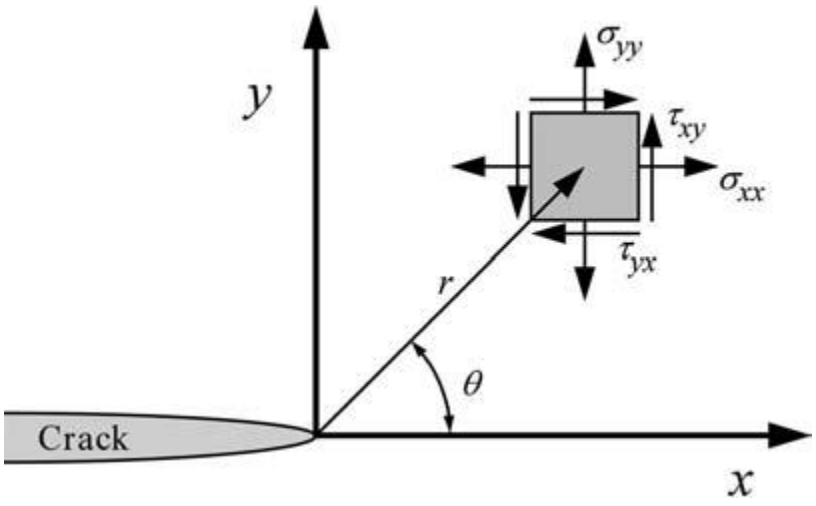

Figure 1.4: Definition of the coordinate axis ahead of a crack tip. The z direction is normal to the page.

For the higher-order terms, A_m is the amplitude $g_{ij}(m)$ and is a dimensionless function of θ for the *m*th term. The higher-order terms depend on geometry, but the solution for any given configuration contains a leading term that is proportional to $1/\sqrt{r}$. As $r \to 0$, the leading term approaches infinity, but the other terms remain finite or approach zero. Thus, stress near the crack tip varies with $1/\sqrt{r}$, regardless of the configuration of the cracked body. It can also be shown that displacement near the crack tip varies with $\sqrt{r}$. Equation (1.1) describes a stress singularity, since stress is asymptotic to $r = 0$.

There are three types of loading that a crack can experience, as Figure. 1.7 illustrates. Mode I loading, where the principal load is applied normal to the crack plane, tends to open the crack. Mode II corresponds to in-plane shear loading and tends to slide one crack face with respect to the other. Mode III refers to out-of-plane shear. A cracked body can be loaded in any one of these

modes, or a combination of two or three modes.

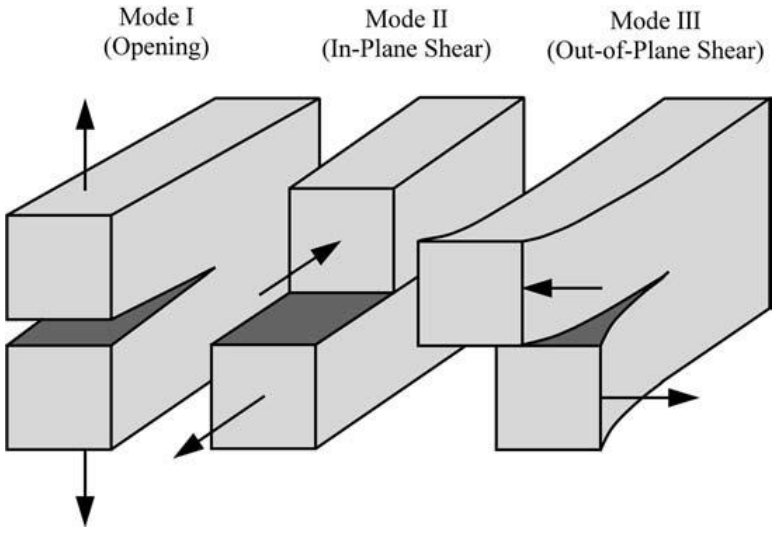

Figure 1.5: The three modes of loading that can be applied to a crack.

1.11.1 The Stress Intensity Factor (SIF)

Each mode of loading produces the $1/\sqrt{r}$ singularity at the crack tip, but the proportionality constants *k* and *fij* depend on the mode. It is convenient at this point to replace *k* by the *stress intensity factor K*, where $K = k\sqrt{2\pi}$. The stress intensity factor is usually given a subscript to

denote the mode of loading, i.e., K_I, K_{II}, or K_{III}. Thus, the stress fields ahead of a crack tip in an isotropic linear elastic material can be written as:

$$\lim_{r\to 0} \sigma_{ij}^{(I)} = \frac{K_I}{\sqrt{2\pi r}} f_{ij}^{(I)}(\theta) \tag{1.2}$$

$$\lim_{r\to 0} \sigma_{ij}^{(II)} = \frac{K_{II}}{\sqrt{2\pi r}} f_{ij}^{(II)}(\theta) \tag{1.3}$$

$$\lim_{r\to 0} \sigma_{ij}^{(III)} = \frac{K_{III}}{\sqrt{2\pi r}} f_{ij}^{(III)}(\theta) \tag{1.4}$$

for Modes I, II, and III, respectively. In a mixed-mode problem (i.e., when more than one loading mode is present), the individual contributions to a given stress component are additive:

$$\sigma_{ij}^{(total)} = \sigma_{ij}^{(I)} + \sigma_{ij}^{(II)} + \sigma_{ij}^{(III)} \tag{1.5}$$

Equation (1.5) stems from the principle of linear superposition.

Detailed expressions for the singular stress fields for Mode I and Mode II are given in Table 1.1. Displacement relationships for Mode I and Mode II are listed in Table 1.2. Table 1.3 lists the nonzero stress and displacement components for Mode III.

Table 1.1: Stress Fields Ahead of a Crack Tip for Mode I and Mode II in a Linear Elastic, Isotropic Material

	Mode I	Mode II
σ_{xx}	$\frac{K_I}{\sqrt{2\pi r}}\cos\left(\frac{\theta}{2}\right)\left[1-\sin\left(\frac{\theta}{2}\right)\sin\left(\frac{3\theta}{2}\right)\right]$	$-\frac{K_{II}}{\sqrt{2\pi r}}\sin\left(\frac{\theta}{2}\right)\left[2+\cos\left(\frac{\theta}{2}\right)\cos\left(\frac{3\theta}{2}\right)\right]$
σ_{yy}	$\frac{K_I}{\sqrt{2\pi r}}\cos\left(\frac{\theta}{2}\right)\left[1+\sin\left(\frac{\theta}{2}\right)\sin\left(\frac{3\theta}{2}\right)\right]$	$\frac{K_{II}}{\sqrt{2\pi r}}\sin\left(\frac{\theta}{2}\right)\cos\left(\frac{\theta}{2}\right)\cos\left(\frac{3\theta}{2}\right)$
τ_{xy}	$\frac{K_I}{\sqrt{2\pi r}}\cos\left(\frac{\theta}{2}\right)\sin\left(\frac{\theta}{2}\right)\cos\left(\frac{3\theta}{2}\right)$	$\frac{K_{II}}{\sqrt{2\pi r}}\cos\left(\frac{\theta}{2}\right)\left[1-\sin\left(\frac{\theta}{2}\right)\sin\left(\frac{3\theta}{2}\right)\right]$
σ_{zz}	0 (Plane stress) $\nu(\sigma_{xx}+\sigma_{yy})$ (Plane strain)	0 (Plane stress) $\nu(\sigma_{xx}+\sigma_{yy})$ (Plane strain)
τ_{xz}, τ_{yz}	0	0

Note: υ is Poisson's ratio.

Table 1.2: Crack-Tip Displacement Fields for Mode I and Mode II (Linear Elastic, Isotropic Material)

	Mode I	Mode II
u_x	$\frac{K_I}{2\mu}\sqrt{\frac{r}{2\pi}}\cos\left(\frac{\theta}{2}\right)\left[\kappa-1+2\sin^2\left(\frac{\theta}{2}\right)\right]$	$\frac{K_{II}}{2\mu}\sqrt{\frac{r}{2\pi}}\sin\left(\frac{\theta}{2}\right)\left[\kappa+1+2\cos^2\left(\frac{\theta}{2}\right)\right]$
u_y	$\frac{K_I}{2\mu}\sqrt{\frac{r}{2\pi}}\sin\left(\frac{\theta}{2}\right)\left[\kappa+1-2\cos^2\left(\frac{\theta}{2}\right)\right]$	$-\frac{K_{II}}{2\mu}\sqrt{\frac{r}{2\pi}}\cos\left(\frac{\theta}{2}\right)\left[\kappa-1-2\sin^2\left(\frac{\theta}{2}\right)\right]$

Note: μ is the shear modulus. $\kappa = 3 - 4\nu$ (plane strain) and $\kappa = (3 - \nu)/(1 + \nu)$ (plane stress).

Table 1.3: Nonzero Stress and Displacement Components in Mode III (Linear Elastic, Isotropic Material)

$$\tau_{xz} = -\frac{K_{III}}{\sqrt{2\pi r}}\sin\left(\frac{\theta}{2}\right)$$

$$\tau_{yz} = \frac{K_{III}}{\sqrt{2\pi r}}\cos\left(\frac{\theta}{2}\right)$$

$$u_z = \frac{2K_{III}}{\mu}\sqrt{\frac{r}{2\pi}}\sin\left(\frac{\theta}{2}\right)$$

Consider the Mode I singular field on the crack plane, where θ = 0. According to Table 1.1, the stresses in the *x* and *y* direction are equal:

$$\sigma_{xx} = \sigma_{yy} = \frac{K_I}{\sqrt{2\pi r}} \quad (1.6)$$

1.12 Conclusions

From a research standpoint, engineers must consider all plausible material failure modes when developing and maturing a new material or when 'evolving' an old material. However, material failure can often be the result of inadequate material selection by the design engineer or their incomplete understanding of the consequences for placing specific types of materials in certain environments.

Education and understanding of the nature of materials and how they fail are essential to preventing it from occurring. Simple fracture or breaking into two pieces is not all-inclusive in terms of failure, because materials also fail by being stretched, dented or worn away. If potential failure modes are understood, then critical systems can be designed with redundancy or with fail-safe features to prevent a catastrophic failure. Furthermore, if appropriate effort is given to understanding the environment and operating loads, keeping in mind potential failure modes, then a system can be designed to be better suited to resist failure.

Chapter II:

The finite element method

2.1 Introduction

The finite element method (FEM) is a numerical method used to solve some of the problems in physics. It is a method which makes it possible to determine an approximate solution over a spatial domain, that is to say which makes it possible to calculate a field (of scalars, vectors, tensors) which corresponds to certain equations and certain imposed conditions.

The method consists in cutting the spatial domain into small elements, also called cells, and in seeking a simplified formulation of the problem on each element, i.e., in transforming the arbitrary system of equations into a system of linear equations. Each system of linear equations can be represented by a matrix. The systems of equations for all the elements are then put together, forming a large matrix; solving this global system gives the approximate solution to the problem.

2.3 Presentation of the finite element method

The analytical resolution of the mechanical problems can be done only in a limited number of cases, however the numerical methods based on the discretization of its problems, present a very effective alternative, often used in the field of mechanics to solve complex problems. The finite element method is the most widely used discretization method because it can deal with complex geometry problems, it covers many areas of physics. Current computer resources (computer power, visualization and simulation tools) make it easy to implement. The finite element method is the most widely used method today, its field of application continues to expand. The success of the method is that its formulation uses standard processes which are repeated during the resolution of problems of different natures. This method is one of the most powerful digital techniques. One of the major advantages of this method is the fact that it offers the possibility of developing a program that can solve, with few modifications, several types of problems. In particular, any complex shape of a geometric domain where a problem is well posed with all the boundary conditions, can be easily treated by the finite element method.

2.4 The outline of the method

In this paragraph, we will try to present in a simplified way, the stages of application of the finite element method and the tools necessary for its implementation.

The resolution of a physical problem by finite elements roughly follows the following steps (Figure. 2.1)

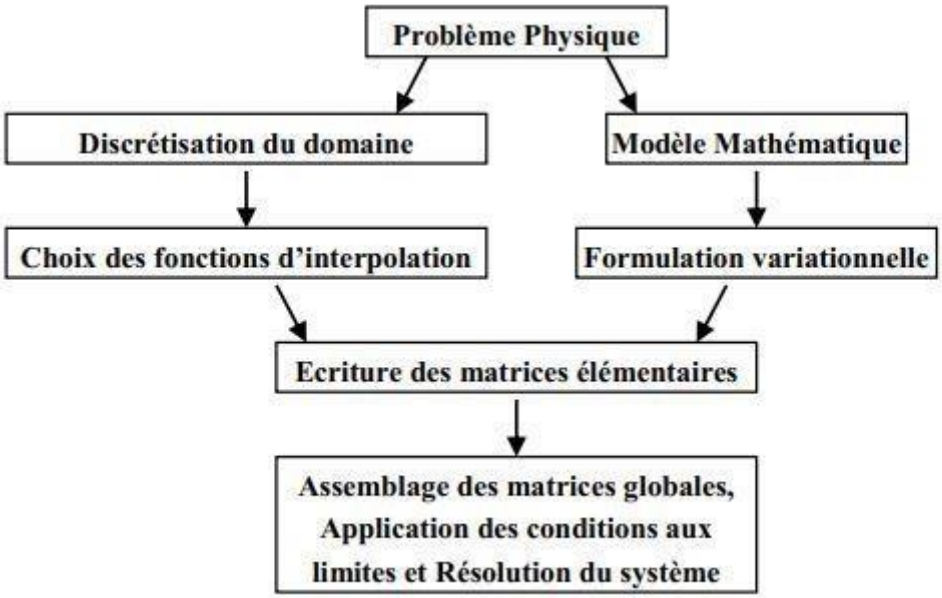

Figure.2.1. General steps of the finite element method

Step 1: Formulation of governing equations and boundary conditions.

The majority of engineering problems are described by partial differential equations associated with boundary conditions defined on a domain and its contour.

The application of the FEM requires a rewriting of these equations in integral form. The weak formulation is often used to include boundary conditions.

Step 2: Division of the domain into subdomains.

This step consists in discretizing the domain into elements and calculating the connectivities of each one as well as the coordinates of its nodes. It thus constitutes the phase of preparation of the geometrical data.

Step 3: Approximation on an element.

In each element the variable such as displacement, pressure, emperature, is approximated by a simple linear, polynomial or other function. The degree of the interpolation polynomial is related to the number of nodes in the element. The nodal approximation is appropriate.

It is in this stage that the construction of the elementary matrices takes place.

Step 4: Assembly and application of boundary conditions.

All the properties of the element (mass, rigidity,) must be assembled in order to form the algebraic system for the nodal values of the physical variables. It is at this level that the connectivities calculated in step 2 are used to build the global matrices from the elementary matrices.

Step 5: Solve the overall system

The overall system can be linear or nonlinear. It can define either a problem of balance, critical values or propagation. The equilibrium problem concerns the static cases and the stationary cases. In a problem of critical values, we are interested in the frequencies and the eigenmodes of vibrations of the physical system studied. Propagation problems concern transient cases in which the variations over time of physical variables are determined.
Stepwise integration methods are better suited for this type of problem. The most used are: central finite difference method, Newmark method, Wilson method

2.5 Classic Element Shapes

There are several forms of classical elements corresponding to one- or three-dimensional domains. Each type of element is identified by a name specifying its shape and by the number of geometric nodes that compose it.

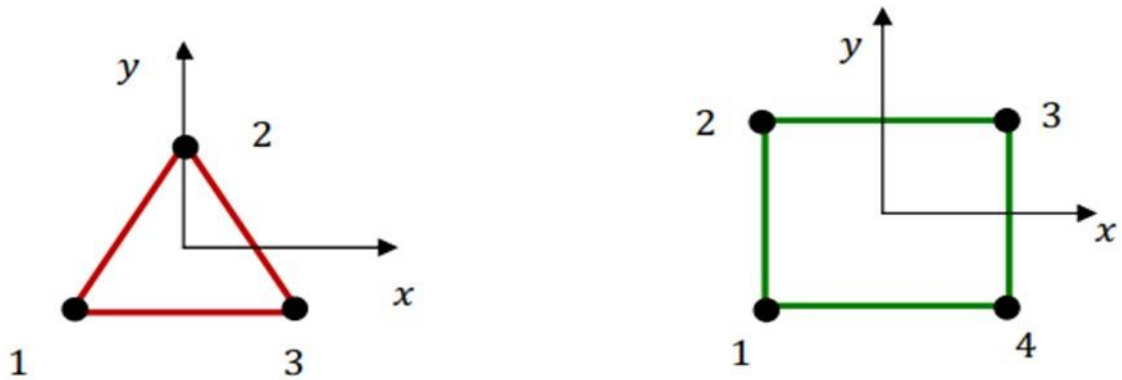

Figure.2.2. Examples of two-dimensional element

2.6 Domain Discretion

The finite element method is an approximation method by sub-domains, so before any application it is necessary to divide the domain to be studied into elements. Each element is geometrically defined by a number of well-defined nodes which generally constitute its vertices (figure.2.2)

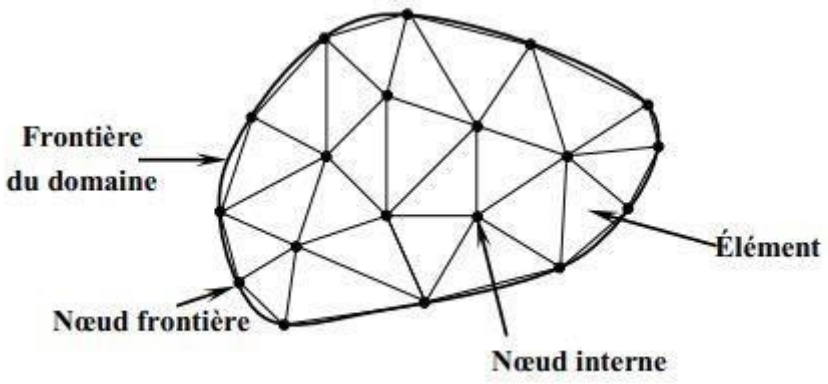

Figure.2.3. Discretization of the domain – triangular elements

The geometric discretization must respect the following rules:

A node of an element must not be inside a side of another of the same type (figure.II.3. a).

No two-dimensional element must be flat, avoid angles close to 180° or 0° (figure.II.3. b).

Two distinct elements can only have in common points located in their common borders (figure.II.3.c).

The set of all elements must constitute a domain as close as possible to the given domain; holes between elements are excluded (figure.2.3. d)

Figure.2.4. Discretization rules

The result of the discretization process must contain two essential data which are the coordinates of the nodes and the connectivities of the elements. One must number all the nodes and the elements so as to have total matrices with small bandwidth, for that, the numbering is done according to the smallest width of the field.

2.7 Use of finite element software

A general industrial-type program must be capable of solving varied large-scale problems (from a thousand to a few hundred thousand variables). These complex programs require a significant approach work before hoping to be able to deal with a real problem in a correct way. Let us cite a few software names by way of example: NASTRAN, ANSYS, ADINA, ABAQUS, CASTEM 2000, CESAR, SAMCEF, etc. The possibilities offered by such programs are numerous:

- linear analysis or not of a continuous physical system.
- static or dynamic analysis.
- taking into account complex behavior laws.
- consideration of various phenomena (elasticity, thermal, electromagnetic, plasticity, flow, etc.) that can be coupled.
- optimization issues, etc..

2.8 Conclusions

We have presented in this chapter the finite element method. The latter is considered among the most powerful and useful methods in numerical calculation, it can facilitate the resolution of rather complex problems. In order to exploit this technique to solve the problem of the cracked structure

Chapter III: Validation by ASME standard

3.1 Introduction

It is obvious that any numerical model produced must be validated by any other method already tested: experimental, analytical, etc. The validation of the proposed methodology using software ANSYS was performed by analytical analysis according ASME requirement. Section XI, Article A-3000, of the ASME Boiler and Pressure Vessel Code provides a method for calculating stress intensity factors (SIFs) K_1 using membrane and bending stresses and it is valid for the calculation of SIFs due to thermal gradients and due to residual stresses. It may be used to calculate SIFs at the deepest point on the crack front and at a point near the free surface. We propose in this part of the work to compare the values of the SIFs calculated from the ANSYS code with those of the analytical method ASME. All calculated values are for the deepest point case. As long as the difference between the two sets of values from the two methodologies is minimal, we can judge that our numerical model is correct.

3.2 Problematic

Irwin introduced in 1948 the concept of the stress intensity factor K very useful in fracture mechanics. [12, 13]. The K describes the singular stress field in the vicinity of the crack. Thus, this factor governs the failure of structures when a critical stress intensity threshold is reached. Around the tip of the crack there is a region where plastic deformation occurs; a finite deformation that leads to damage. Consequently, the stresses do not follow just the singular stress term inside this region and generally are leveled off due to damage of the material.

This approach requires that constraint in the test specimen approximate that of the structure to provide an “effective” toughness for use in a structural integrity assessment. The appropriate constraint is achieved by matching thickness and crack depth between specimen and structure. Experimental studies [13, 14] demonstrate the validity of this approach. These studies show that the use of geometry dependent fracture toughness values allows more accurate prediction of the fracture performance of structures then it is possible to conventional fracture mechanics. Linear elastic fracture mechanics provides the relationships between the applied stress, the fracture toughness of the material and the critical crack size.

Appendix D ASME VIII Div 3 provides engineering methods for calculating the stress intensity factor K_I for various postulated crack geometries in thick-walled vessels.

In this work, we will be interested, more particularly, in the investigation of the effect of the ratio of the depth of the crack on the thickness of the vessel (a/t) and the effect of the ratio of the geometry of the crack (a/c) on the SIF (Figure. 1). The analysis of the SIF is done under the

assumption that the propagation is done radially (according to the thickness of the enclosure), and uses, also the assumption of the infinite plate with a uniaxial stress field, then that in reality it is a triaxial field.

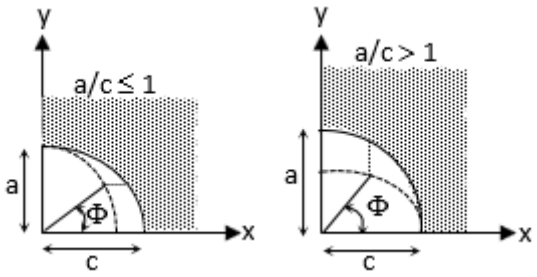

Figure 2.1: Surface crack in a finite plate

3.3 Eccentric angle and Parametric equations of an ellipse

Let P be any point on the ellipse. Draw PN perpendicular to the major axis and produce it to meet the auxiliary circle at Q. Then angle ACQ is called the 'eccentric angle' of the point P. Let us denote the angle as θ. If P starts from A and moves along the ellipse in the anti-clock wise direction and comes once again at A, then θ will vary from 0 to 2π. Let the coordinates of P be (x, y).

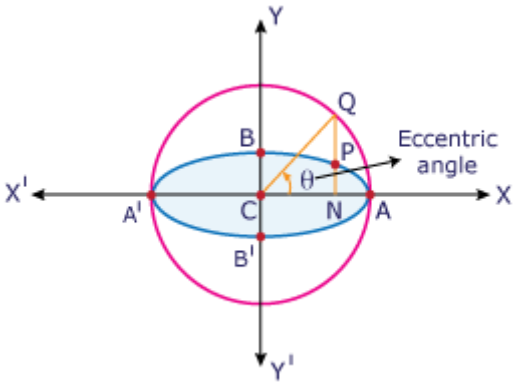

hen x = a cos θ

[∵ from Δ CNQ, cos θ = x/a where CQ is the radius of the auxiliary circle]

Since P lies on the ellipse $\frac{x^2}{a^2}+\frac{y^2}{b^2}=1$

we have $\frac{a^2cos^2\theta}{a^2}+\frac{y^2}{b^2}=1$

$y^2=b^2$ (1 – cos2 θ)

$=b^2$ sin2 θ

Y=b sin θ

The coordinates of P are (a cos θ, b sin θ).

The point (a cos θ, b sin θ) is, for the sake of brevity, called the point θ and is denoted by P(θ).

If we put x = a cos θ, y = b sin θ in the equation of the ellipse, the equation is satisfied for all values of θ. Hence the pair of equations x = a cos θ, y = b sin θ together yield the single equation $\frac{x^2}{a^2} + \frac{y^2}{b^2} = 1$

The two equations x = a cos θ, y = b sin θ are known as the parametric equations of the ellipse and 'θ' is called the parameter.

3.4 Verification methods of numerical approach

There are several methods for developing SIF solutions for cracked structure problems [15, 16]. Basic solutions for simple geometries can be derived using classical elasticity methods that employ complex stress functions [15, 17]. There are also several experimental methods that have been used to obtain (or verify) the SIF for cracked structural elements, i.e., the compliance method and the photo-elastic method. While a general knowledge of each SIF solution method might be useful for undertaking specific problems, detailed knowledge is required before any method can be applied to solve a given problem.

This method may be used to calculate stress intensity factors for cracks of type A (Figure. 2). The same method is also valid for the calculation of stress intensity factors due to thermal gradients and due to residual stresses [18]. It may be used to calculate stress intensity factors at the deepest point on the crack front and at a point near the free surface. For a surface flaw, the stresses normal to the plane of the flaw at the flaw location are represented by a polynomial fit over the flaw depth by the following Relationship:

$$\sigma = A_0 + A_1(x/a) + A_2(x/a)^2 + A_3(x/a)^3 \quad (2.1)$$

Where:

A_0, A_1, A_2, A_3 are constants;

a, crack depth;

x, distance through the wall measured from the flawed surface.

Coefficients A_0 through A_3 shall provide an accurate representation of stress over the flaw plane for all (Figure. 2.3)

Values of flaw depths, $0 \leq x/a \leq 1$, covered by the analysis. Stresses from all sources shall be considered.

Stress intensity factors for surface flaws shall be calculated using the cubic polynomial stress relation given by Eq. (2.2):

$$K_1 = \left[(A_0 + A_p)G_0 + A_1G_1 + A_2G_2 + A_3G_3\right]\sqrt{\pi\, a/Q} \quad (2.2)$$

Where:

A_0, A_1, A_2, A_3 , coefficients from Eq. (2.1) that represent the stress distribution over the flaw depth, $0 \leq x/a \leq 1$.

When calculating K_I as a function of flaw depth, a new set of coefficients A_0 through A3 shall be determined for each new value of flaw depth.

A_p, internal vessel pressure p, if the pressure acts on the crack surfaces ($A_p = 0$ for other flaws.

G_0, G_1, G_2, G_3, free surface correction factors from Tables 2.1, The values of the coefficients for the case of the free surface are given in appendix A.

Q, flaw shape parameter using Eq. (2.3)

$$Q = 1 + 4.593(a/2c)^{1.65} - q_y \qquad (2.3)$$

Where:

$l = 2c$, major axis of the flaw;

a/l, flaw aspect ratio $0 \leq a/ø \leq 0.5$;

q_y, plastic zone correction factor and in our case its neglected

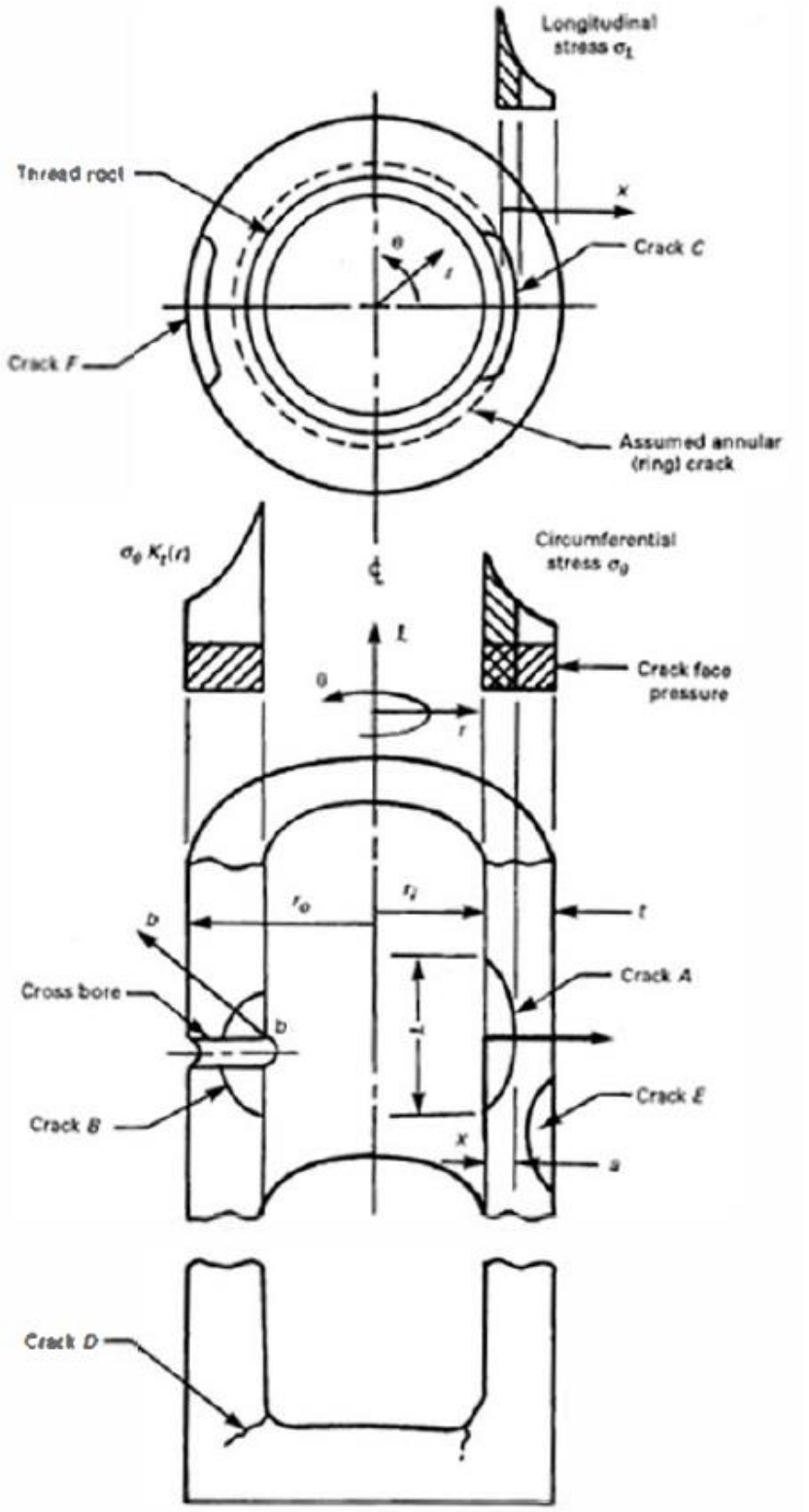

Figure 2.2: Cracks types [18]

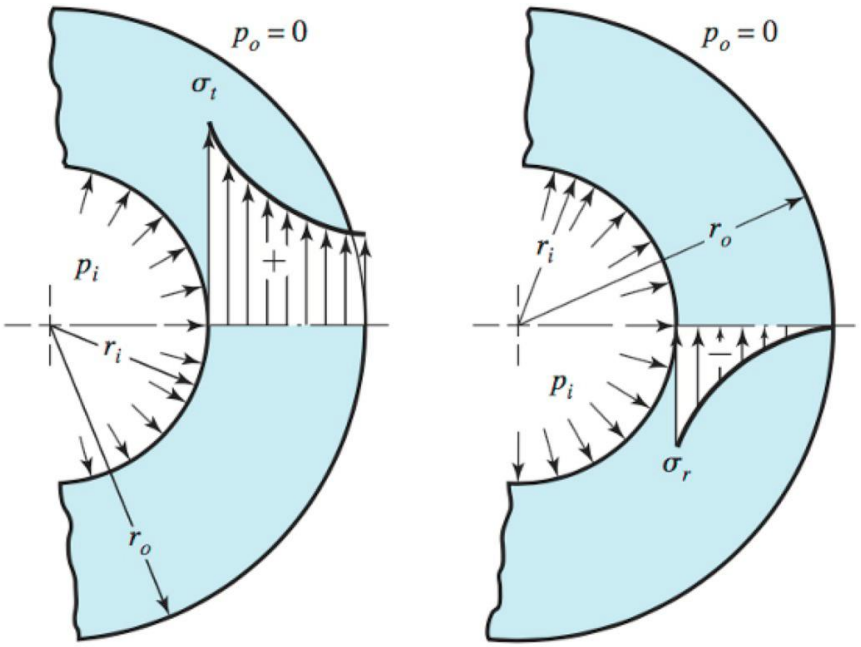

Figure 2.3: Hoop and radial stress distribution in a pressure vessel

Table 2.1: Coefficients G_0 through G_3 for surface crack at deepest point [18]

Coefficients	a/t	Flaw Aspect Ratio a/2c					
		0.0	0.1	0.2	0.3	0.4	0.5
Uniform	**0.00**	1.1208	1.0969	1.0856	1.0727	1.0564	1.0366
G0	**0.05**	1.1461	1.1000	1.0879	1.0740	1.0575	1.0373
	0.10	1.1945	1.1152	1.0947	1.0779	1.0609	1.0396
	0.15	1.2670	1.1402	1.1058	1.0842	1.0664	1.0432
	0.20	1.3654	1.1744	1.1210	1.0928	1.0739	1.0482
	0.25	1.4929	1.2170	1.1399	1.1035	1.0832	1.0543
	0.30	1.6539	1.2670	1.1621	1.1160	1.0960	1.0614
	0.40	2.1068	1.3840	1.2135	1.1448	1.1190	1.0772
	0.50	2.8254	1.5128	1.2693	1.1757	1.1457	1.0931
	0.60	4.0420	1.6372	1.3216	1.2039	1.1699	1.1058
	0.70	6.3743	1.7373	1.3610	1.2237	1.1868	1.1112
	0.80	11.9910	1.7899	1.3761	1.2285	1.1902	1.1045
Linear	**0.00**	0.7622	0.6635	0.6826	0.7019	0.7214	0.7411
G1	**0.05**	0.7624	0.6651	0.6833	0.7022	0.7216	0.7413
	0.10	0.7732	0.6700	0.6855	0.7031	0.7221	0.7418
	0.15	0.7945	0.6780	0.6890	0.7046	0.7230	0.7426
	0.20	0.8267	0.6891	0.6939	0.7067	0.7243	0.7420
	0.25	0.8706	0.7029	0.7000	0.7094	0.7260	0.7451
	0.30	0.9276	0.7193	0.7073	0.7126	0.7282	0.7468
	0.40	1.0907	0.7584	0.7249	0.7209	0.7338	0.7511
	0.50	1.3501	0.8029	0.7454	0.7314	0.7417	0.7566
	0.60	1.7863	0.8488	0.7671	0.7441	0.7520	0.7631
	0.70	2.6125	0.8908	0.7882	0.7588	0.7653	0.7707
	0.80	4.5727	0.9288	0.8063	0.7753	0.7822	0.7792
Quadratic	**0.00**	0.6009	0.5078	0.5310	0.5556	0.5815	0.6084
G2	**0.05**	0.5969	0.5086	0.5313	0.5557	0.5815	0.6084
	0.10	0.5996	0.5109	0.5323	0.5560	0.5815	0.6085
	0.15	0.6088	0.5148	0.5340	0.5564	0.5815	0.6087
	0.20	0.6247	0.5202	0.5364	0.5571	0.5815	0.6089
	0.25	0.6475	0.5269	0.5394	0.5580	0.5817	0.6093
	0.30	0.6775	0.5350	0.5430	0.5592	0.5820	0.6099
	0.40	0.7651	0.5545	0.5520	0.5627	0.5835	0.6115
	0.50	0.9048	0.5776	0.5632	0.5680	0.5869	0.6144
	0.60	1.1382	0.6027	0.5762	0.5760	0.5931	0.6188
	0.70	1.5757	0.6281	0.5907	0.5874	0.6037	0.6255
	0.80	2.5997	0.6513	0.6063	0.6031	0.6200	0.6351
Cubic	**0.00**	0.5060	0.4246	0.4480	0.4735	0.5006	0.5290
G3	**0.05**	0.5012	0.4250	0.4482	0.4736	0.5006	0.5290
	0.10	0.5012	0.4264	0.4488	0.4736	0.5004	0.5290
	0.15	0.5059	0.4286	0.4498	0.4737	0.5001	0.5289
	0.20	0.5152	0.4317	0.4511	0.4738	0.4998	0.5289
	0.25	0.5292	0.4357	0.4528	0.4741	0.4994	0.5289
	0.30	0.5483	0.4404	0.4550	0.4746	0.4992	0.5291
	0.40	0.6045	0.4522	0.4605	0.4763	0.4993	0.5298
	0.50	0.6943	0.4665	0.4678	0.4795	0.5010	0.5316
	0.60	0.8435	0.4829	0.4769	0.4853	0.5054	0.5349
	0.70	1.1207	0.5007	0.4880	0.4945	0.5141	0.5407
	0.80	1.7614	0.5190	0.5013	0.5085	0.5286	0.5487

3.5 Results and discussions

The SIF values calculated from the analytical method of the ASME standard and those obtained by the finite element method (ANSYS) are presented in tables 2.2-4. SIF results are given for different crack shapes (a/c = 0.2 to 1) and for different crack sizes (a/t = 0.25 to 0.8).

Table 2.2: K_I values (MPa√m) calculated by ASME and ANSYS at deepest point (a/t =0.25)

a/c	ASME	ANSYS	Deviation
0.2	55.62	54.50	2.01
0.4	47.56	46.62	1.97
0.6	41.46	40.60	2.07
0.8	36.62	36.52	0.26
1	32.20	36.19	12.37

Table 2.3: KI values (MPa√m) calculated by ASME and ANSYS at deepest point (a/t =0.4)

a/c	ASME	ANSYS	Deviation
0.2	79.80	77.90	2.38
0.4	63.85	62.74	1.73
0.6	54.23	53.16	1.99
0.8	47.69	48.47	1.65
1	41.48	47.46	14.43

Table 2.4: KI values (MPa√m) calculated by ASME and ANSYS at deepest point (a/t =0.8)

a/c	ASME	ANSYS	Deviation
0.2	144.97	149.19	2.91
0.4	101.58	102.48	0.88
0.6	81.59	88.71	8.73
0.8	71.08	82.86	16.57
1	59.54	77.61	30.34

Figures 2.4-6 represent the evolution of SIF as a function of crack shape (a/c) for the three crack sizes a/t=0.25, 0.4 and 0.8 respectively. It is noted that the SIF values resulting from the two methods are almost identical except for the value of a/c = 1 (circular crack). The ASME standard stipulates that the procedure is not valid for the case of the circular crack (a/c=1) [19]. The results found show the accuracy of our elaborate numerical model. This gives us confidence to calculate the rest of the SIF values for the different parametric angles (Φ=0 to 180°).

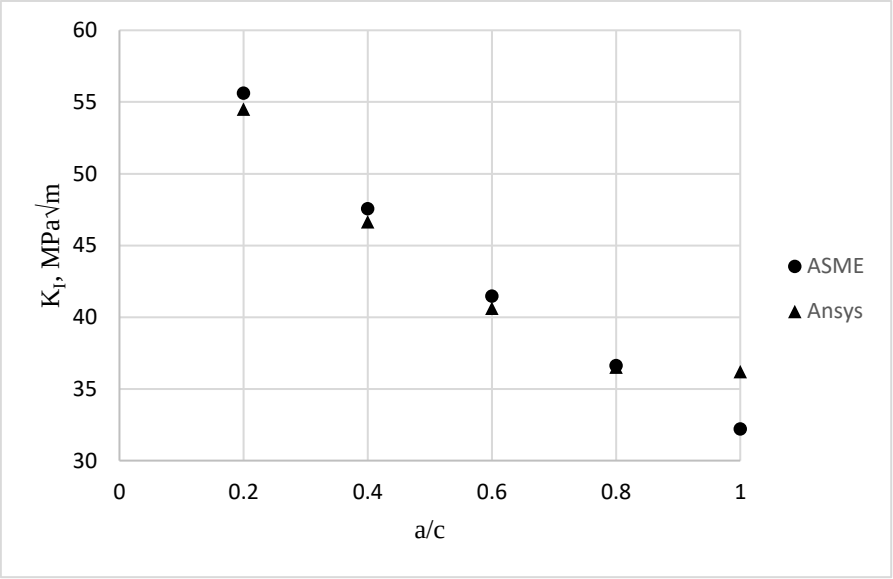

Figure 2.4: SIF values for deepest point (a/t = 0.25)

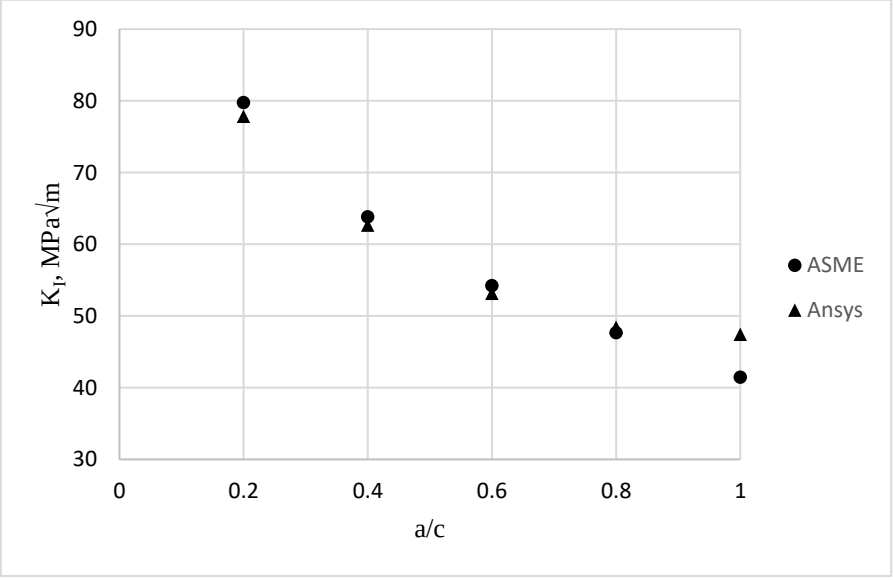

Figure 2.5: SIF values for deepest point (a/t = 0.4)

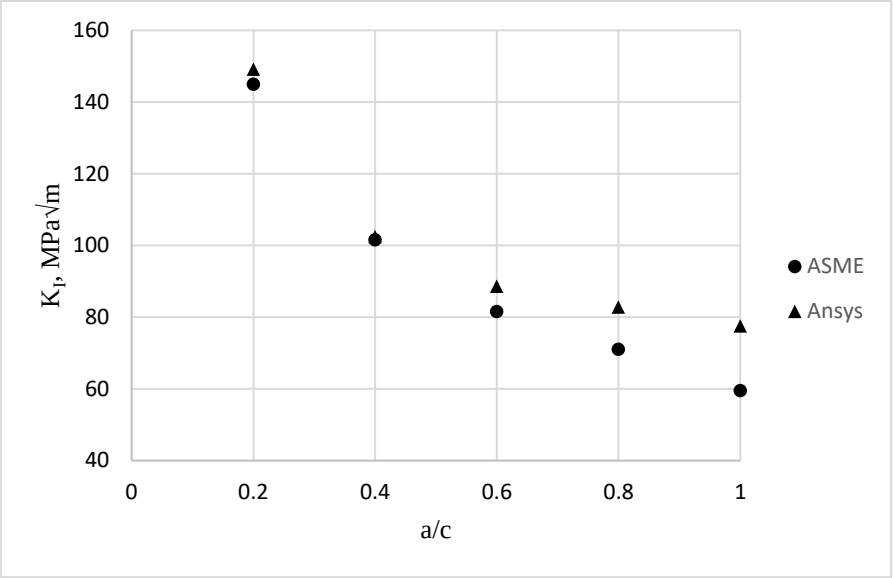

Figure 2.6: SIF values for deepest point (a/t = 0.8)

3.6 Conclusions

A numerical model has been proposed for the calculation of SIF for longitudinal semi-elliptical cracks located in the wall of a pressure vessel. The model has been validated by the ASME standard.

The results obtained show good agreement with those reported in the literature. They show that the SIF depends on the ratios a/c and a/t, as it depends on the parametric angle Φ. These results also show that SIF calculations based on the simplistic infinite plate assumption give lower values than reality, because they misrepresent the stress distribution with respect to the crack extent.

As it has already been said previously that the ASME procedure is only valid for two parametric angles Φ=0 and Φ=90. In chapter 3 we will calculate the SIF for an angle varying between 0° and 180° and this for the different shapes of the crack (a/c) and for the different sizes of the crack (a/t).

Chapter IIII: Analysis of a longitudinal crack developing in the vessel pressure wall

4.1 Introduction

In the design of pressure vessel, the use of fracture mechanics theory and non-destructive testing are the most effective tools for design engineers. Fracture mechanics is generally used to predict the failure of components caused by the preexistence of small cracks. It also allows us to take our precautions to stop any future propagation of the crack or to determine the life of the structure in the event that propagation is unavoidable.

In the case of an elastic material (brittle fracture), one of the most used cracking criteria is the stress intensity factor (SIF). However, and because it is difficult to accurately determine the SIF for cracks in complex structures by analytical solutions, the use of numerical methods such as finite elements become the only appropriate tool [20, 21].

In this work we will proceed to the calculation of the SIF in the vessel pressure wall, we will be interested, more particularly, in the investigation of the effect of the ratio of the depth of the crack on the thickness of the vessel (a/t) and the effect of the ratio of the geometry of the crack (a/c) on the SIF. The analysis of the SIF is done under the assumption that the propagation takes place radially (according to the thickness of the vessel) subject to a triaxial stress field.

4.2 Numerical model description

Finite element (FE) analysis is performed using ANSYS 2022R1 code. The developed Workbench 2022R1 model is shown in Figure. 1. 3D finite element model of pressure vessel with crack was prepared for SIF modelling. As the pressure vessel is symmetric only 1/12 of the component was modeled (Figure. 2) The prepared FE model with applied pressure and boundary conditions is shown in Figure. 3. Symmetry boundary conditions were applied to all four edge surfaces. A pressure of 8.25 MPa was applied to the inner vessel.

The ANSYS code adopts two approaches for the evaluation of SIFs:

- Contour integral method: the calculation of the SIF is performed during the solving phase and the results are stored for post-processing.
- Displacement extrapolation method: the calculation of the SIF is performed during post-processing. This method is limited to linear elasticity problems with homogeneous isotropic materials near the crack region.

The contour integral method is suitable for a wide range of applications. In finite element analysis, this method is suitably accurate for the evaluation of mixed-mode SIF and it is also a robust tool for heterogeneous models with continuous, discontinuous or nonlinear material properties. This method gives more accurate results because the contour integral is evaluated at points away from the crack. In our study, we used the contour integral method.

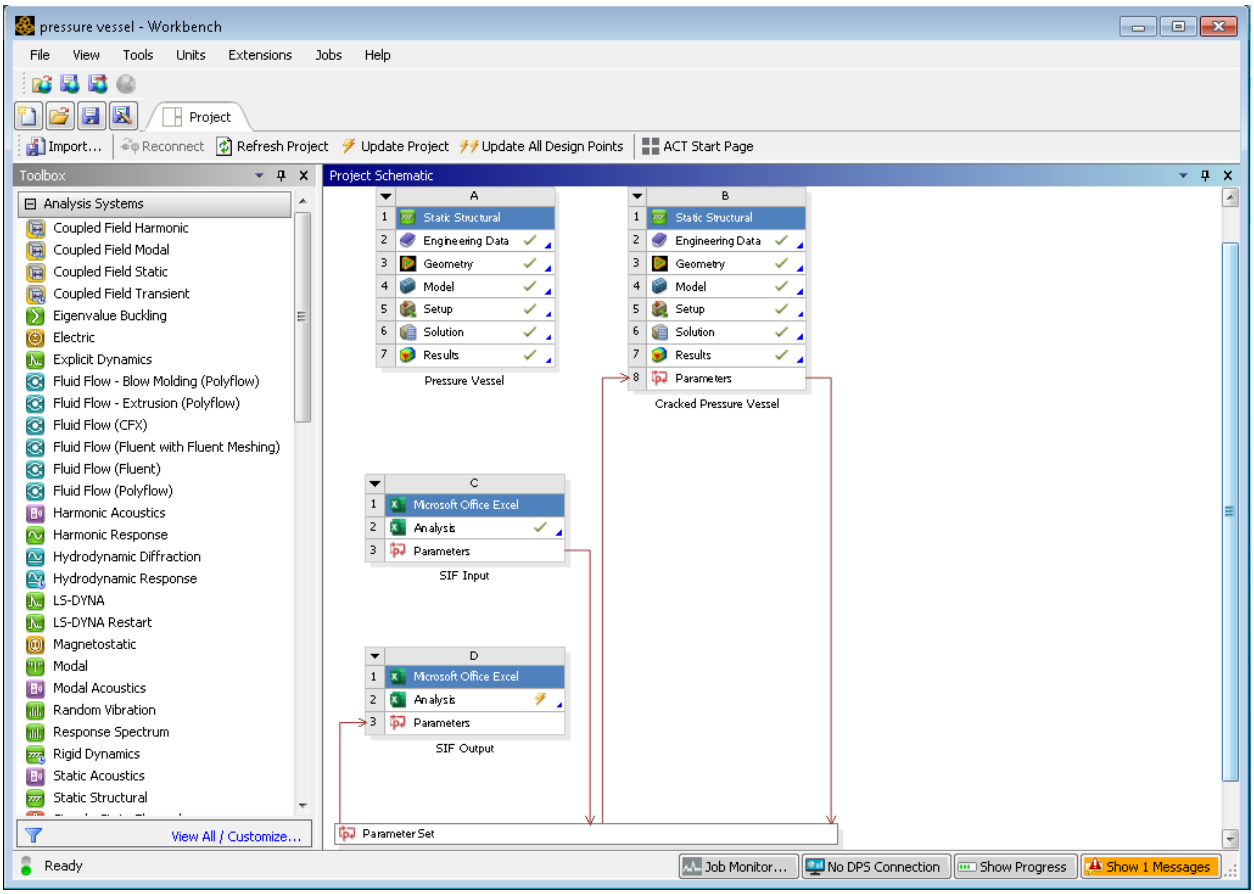

Figure 3.1: Workbench 2022R1 model

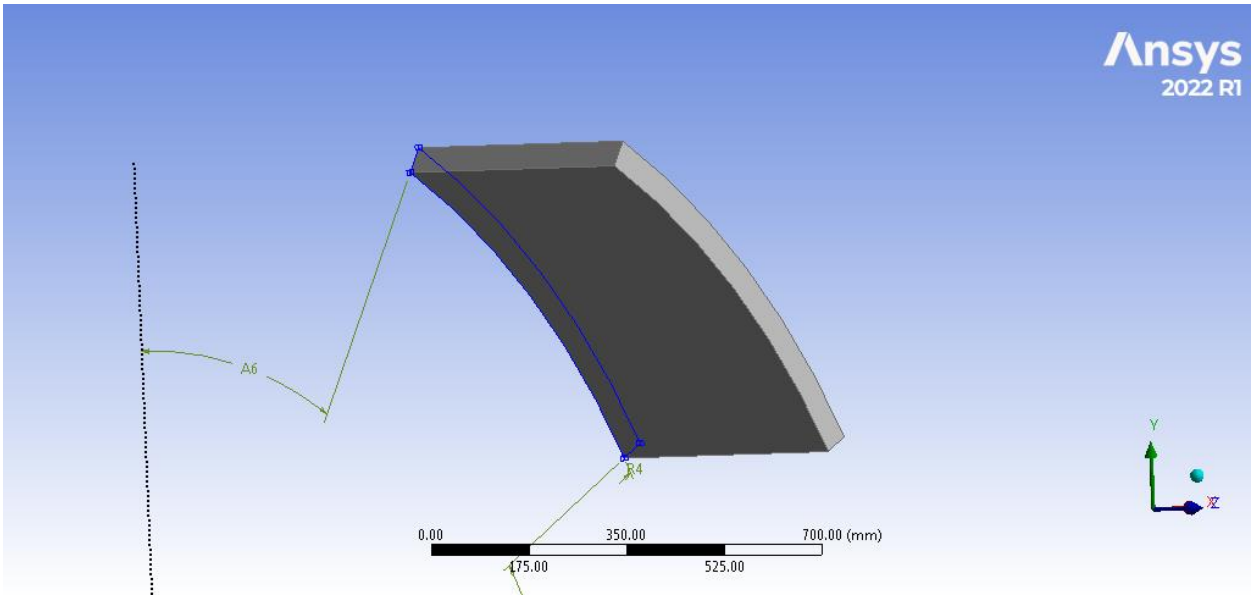

Figure 3.2: FE model of 1/12 of vessel pressure vessel with applied boundary conditions and load prepared with ANSYS.

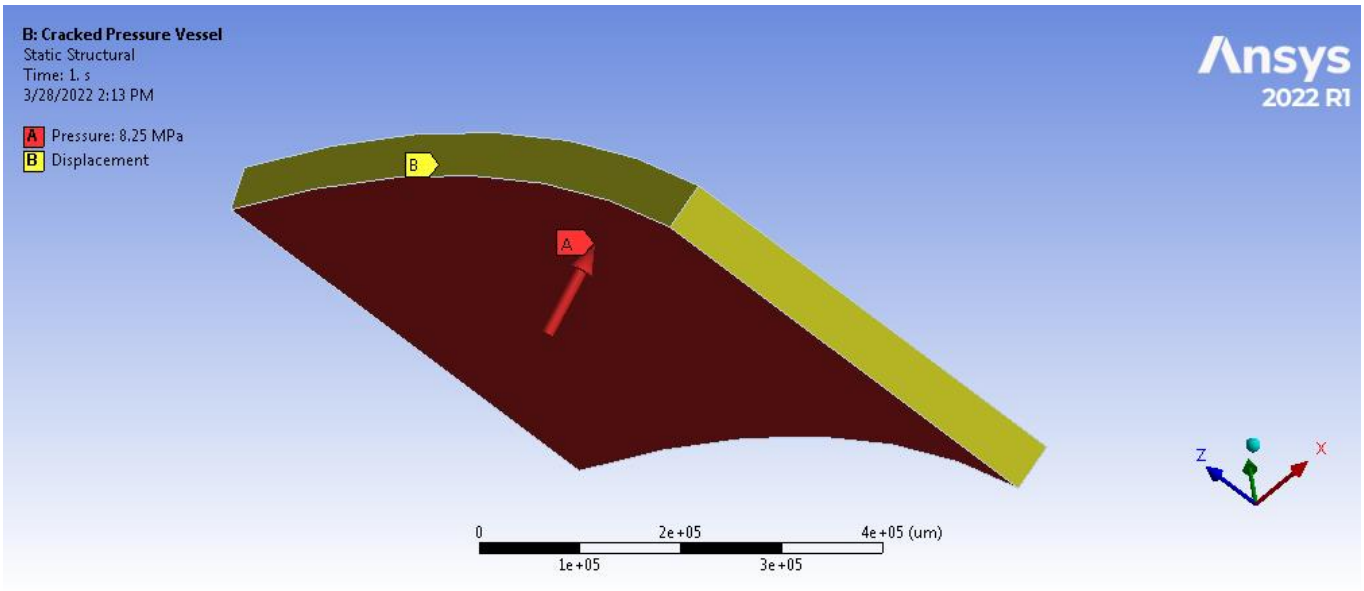

Figure 3.3: Load applied and boundary conditions

The main configurations used by ANSYS in the rupture module are (Figure. 4):

a. **Major Radius**: Specifies the major radius, which defines the size of the crack shape along the Z axis (that is, the width of the crack "c").

b. **Minor Radius**: Specifies the minor radius, which defines the size of the crack shape along the X axis (that is, the depth of the crack "a").

c. **Mesh Method**: This property enables us to select the mesh method to be used to mesh the semi-elliptical crack. Options include Hex Dominant (default) and Tetrahedrons.

d. **Largest Contour Radius**: Specifies the largest contour radius for the crack shape.

e. **Crack Front Divisions:** Specifies the number of divisions for the crack front.

f. **Fracture Affected Zone:** The fracture affected zone is the region that contains a crack. The Fracture Affected Zone control determines how the fracture affected zone height is defined:

   - Program Controlled: The software calculates the height, and Fracture Affected Zone Height is read-only. This is the default.
   - Manual: You enter the height in the Fracture Affected Zone Height field.

g. **Fracture Affected Zone Height**: This value specifies two things: 1) the height of the Fracture Affected Zone, which is in the Y direction of the crack coordinate system; and 2) the distance in totality by which the Fracture Affected Zone is extended in the positive and negative Z direction of the crack coordinate system from the crack front extremities.

h. **Circumferential Divisions**: Specifies the number of circumferential divisions for the crack shape.

i. **Mesh Contours**: Specifies the number of mesh contours for the crack shape.

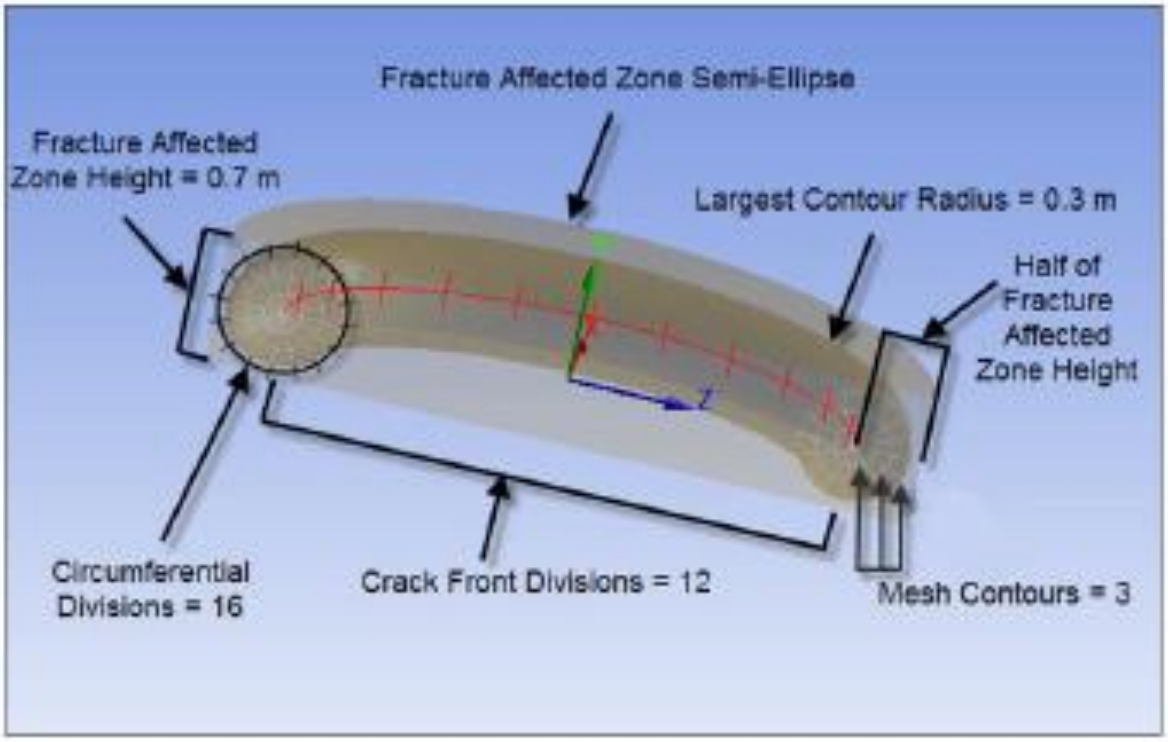

Figure 3.4: The different configuration parameters of the semi-elliptical crack [22]

Table 1 summarizes the analyzed crack geometries. For each crack geometry of the fifteen analyzed cases, a configuration of the crack parameters is introduced (crack front division, circumferential division, mesh contours, etc).

Table 3.1: The different shapes of cracks analyzed

a/c	**0.2**	**0.4**	**0.6**	**0.8**	**1**	
a [mm]			**c [mm]**			**a/t**
12.5	62.5	31.25	20.83	15.62	12.5	**0.25**
20	100	50	33.33	25	20	**0.4**
40	200	100	66.66	50	40	**0.8**

Figure 3.5 shows the refinement of the mesh around the crack.

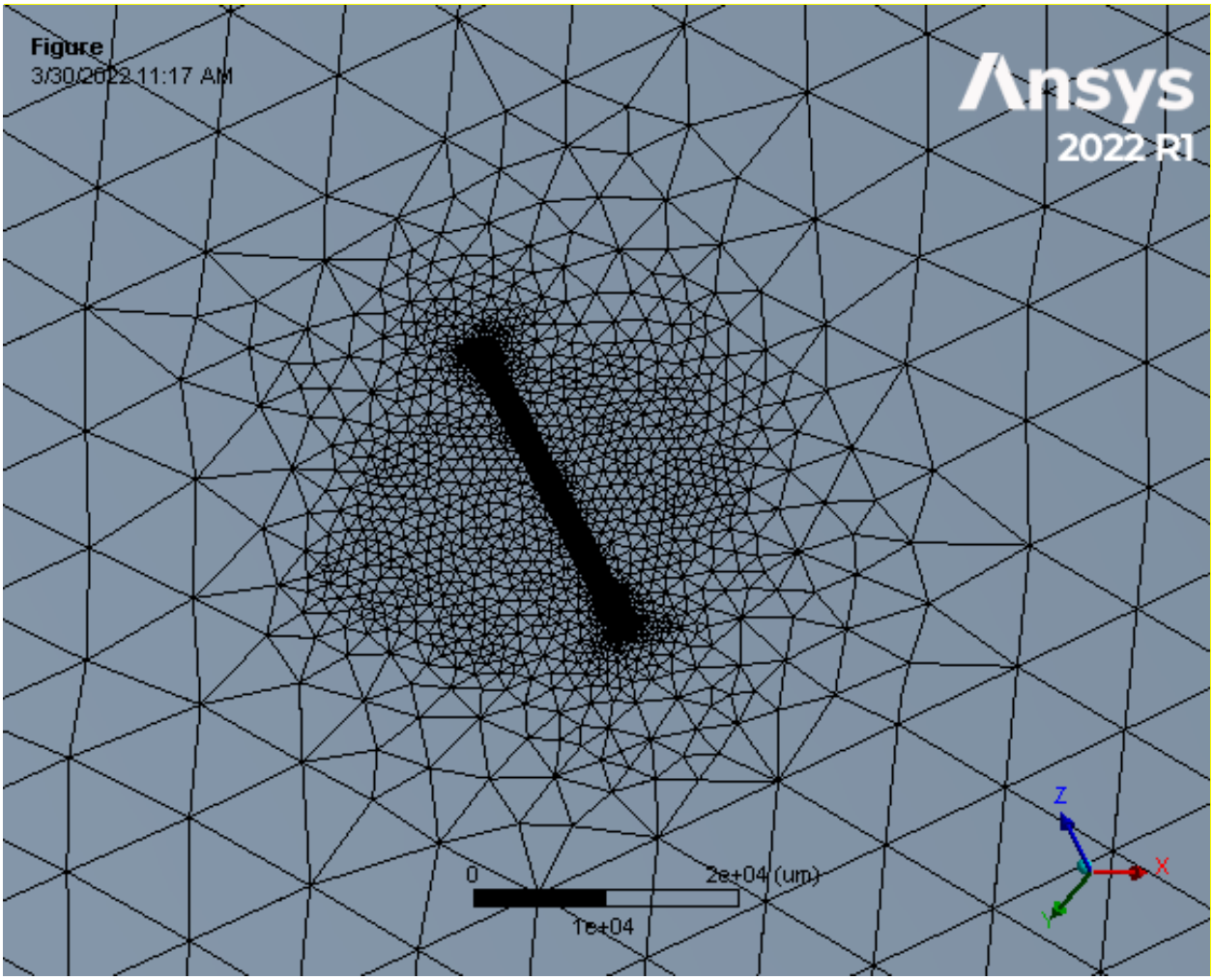

Figure 3.5: Refinement mesh around the crack

4.3 Results and discussions

Figures 3.6-8 show the evolution of SIF as a function of the parametric angle Φ for crack sizes (a/t) equal 0.25, 0.4 and 0.8 respectively. The first observation is that the value of the SIF increases with the size of the crack (a/t). It is also observed that the maximum stress-intensity factor occurs at the maximum depth point for small ratios of crack depth to crack length (a/c) and at the intersection of the crack with the front surface for large ratios. As one approaches the circular shape (a/c=1), the maximum of the SIF shifts towards the free surface (intersection of the crack with the wall). This result is consistent with several previous studies, including that of J. C. Newman [19]. From these figures, it can be seen that the crack propagates along the semi-elliptical trajectory.

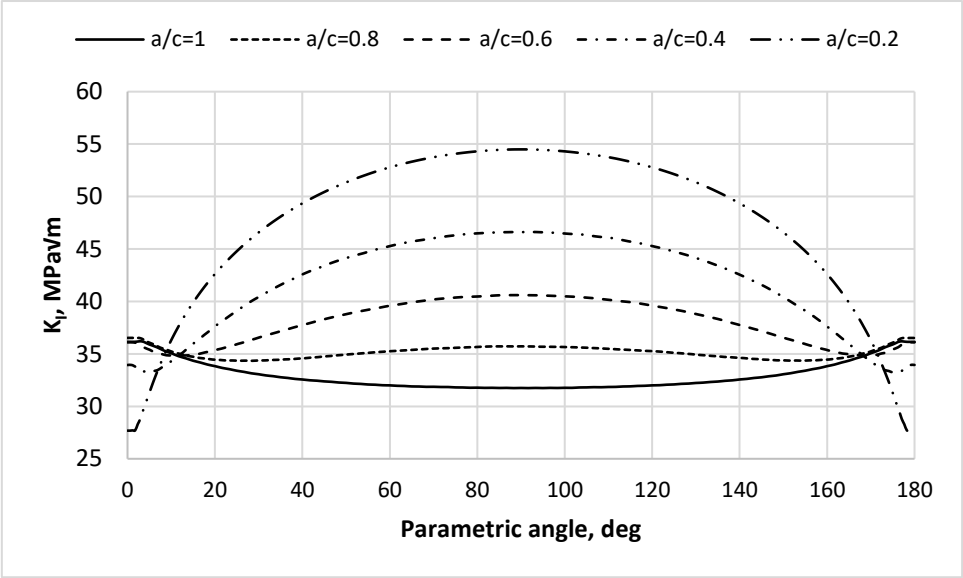

Figure 3.6: KI values depending on the parametric angle Φ (a/t =0.25)

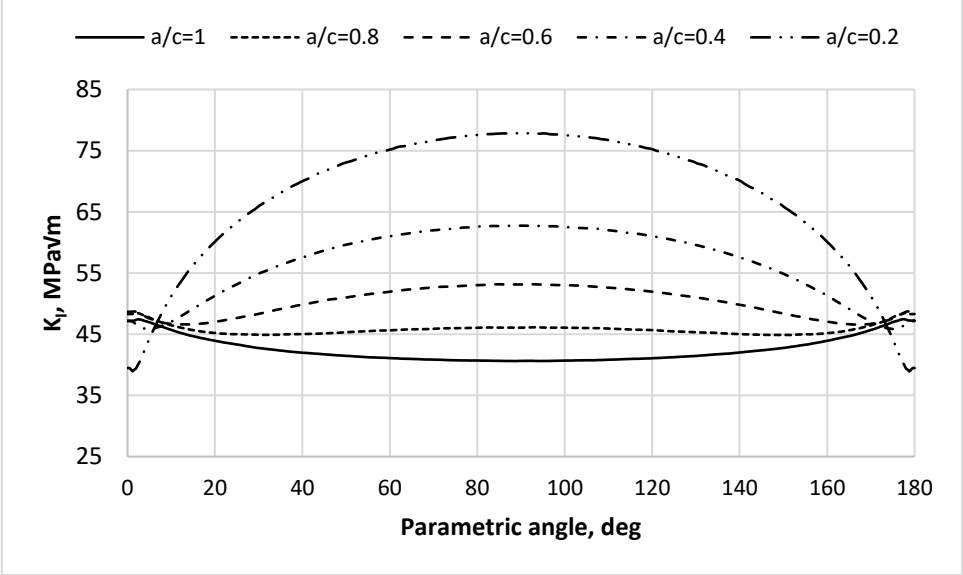

Figure 3.7: KI values depending on the parametric angle Φ (a/t =0.4)

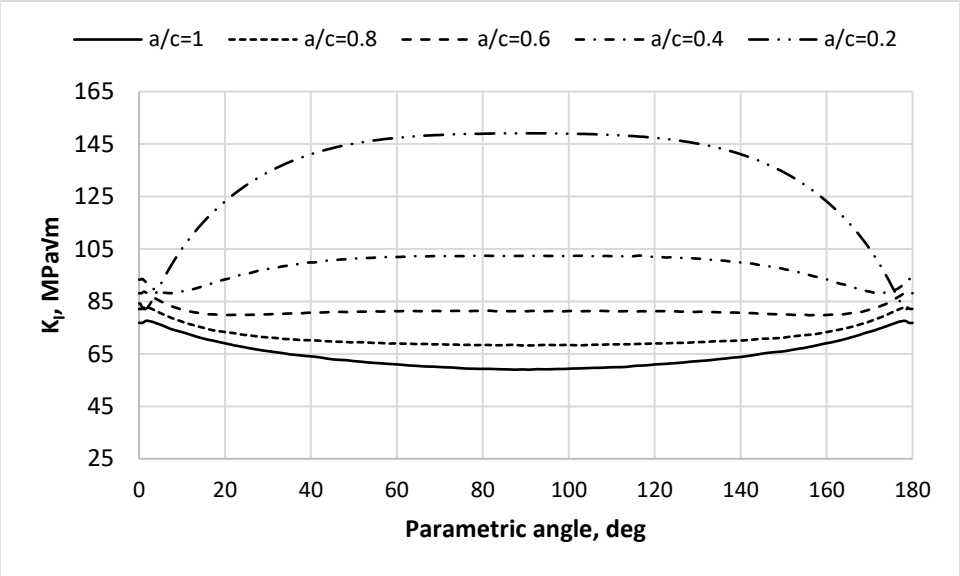

Figure 3.8: KI values depending on the parametric angle Φ (a/t =0.8)

4.5 Conclusions

A three-dimensional, finite-element stress analysis was used to calculate mode I stress-intensity factor variations along the crack front for a wide range of semielliptical surface cracks in vessel pressure subjected to inner pressure. The maximum stress-intensity factor occurs at the maximum depth point for small ratios of crack depth to crack length and at the intersection of the crack with the front surface for large ratios.

General conclusions

Longitudinal cracks that can develop in pressure vessels are a critical hazard. These cracks are generally born in the discontinuities of the structure such as the weld joint. Through this study, a three-dimensional numerical model, using ANSYS software, is proposed for the calculation of the stress intensity factor (SIF) along the longitudinal semi-elliptical crack tip located in the wall of a pressure vessel.

The validation of the proposed methodology using software ANSYS was performed by analytical analysis according ASME requirement. Section XI, Article A-3000, of the ASME Boiler and Pressure Vessel Code provides a method for calculating stress intensity factors K I using membrane and bending stresses and it is valid for the calculation of SIFs due to thermal gradients and due to residual stresses.

The results showed that the maximum stress-intensity factor occurs at the maximum depth point for small ratios of crack depth to crack length and at the intersection of the crack with the front surface for large ratios.

The results show good agreement with those reported in the literature. They show that the SIF depends on the ratios a/c and a/t, as it depends on the parametric angle Φ. These results also show that SIF calculations based on the simplistic infinite plate assumption give lower values than reality, because they misrepresent the stress distribution with respect to the crack extent.

Appendix A: Coefficients G0 through G3 for surface crack at free surface

Coefficient	a/t	Flaw Aspect Ratio a/2c					
		0.0	**0.1**	**0.2**	**0.3**	**0.4**	**0.5**
Uniform	**0.00**	0.0000	0.5450	0.7492	0.9024	1.0297	1.1406
G0	**0.05**	0.0000	0.5514	0.7549	0.9070	1.0330	1.1427
	0.10	0.0000	0.5610	0.7636	0.9144	1.0391	1.1473
	0.15	0.0000	0.5738	0.7756	0.9249	1.0479	1.1545
	0.20	0.0000	0.5900	0.7908	0.9385	1.0596	1.1641
	0.25	0.0000	0.6099	0.8095	0.9551	1.0740	1.1763
	0.30	0.0000	0.6338	0.8318	0.9750	1.0913	1.1909
	0.40	0.0000	0.6949	0.8881	1.0250	1.1347	1.2278
	0.50	0.0000	0.7772	0.9619	1.0896	1.1902	1.2746
	0.60	0.0000	0.8859	1.0560	1.1701	1.2585	1.3315
	0.70	0.0000	1.0283	1.1740	1.2686	1.3401	1.3984
	0.80	0.0000	1.2144	1.3208	1.3871	1.4361	1.4753
Linear	**0.00**	0.0000	0.0725	0.1038	0.1280	0.1484	0.1665
G1	**0.05**	0.0000	0.0744	0.1075	0.1331	0.1548	0.1740
	0.10	0.0000	0.0771	0.1119	0.1387	0.1615	0.1816
	0.15	0.0000	0.0807	0.1169	0.1449	0.1685	0.1893
	0.20	0.0000	0.0852	0.1227	0.1515	0.1757	0.1971
	0.25	0.0000	0.0907	0.1293	0.1587	0.1833	0.2049
	0.30	0.0000	0.0973	0.1367	0.1664	0.1912	0.2128
	0.40	0.0000	0.1141	0.1544	0.1839	0.2081	0.2289
	0.50	0.0000	0.1373	0.1765	0.2042	0.2265	0.2453
	0.60	0.0000	0.1689	0.2041	0.2280	0.2466	0.2620
	0.70	0.0000	0.2121	0.2388	0.2558	0.2687	0.2791
	0.80	0.0000	0.2714	0.2824	0.2887	0.2931	0.2965
Quadratic	**0.00**	0.0000	0.0254	0.0344	0.0423	0.0495	0.0563
G2	**0.05**	0.0000	0.0264	0.0367	0.0456	0.0538	0.0615
	0.10	0.0000	0.0276	0.0392	0.0491	0.0582	0.0666
	0.15	0.0000	0.0293	0.0419	0.0527	0.0625	0.0716
	0.20	0.0000	0.0313	0.0450	0.0565	0.0669	0.0764
	0.25	0.0000	0.0338	0.0484	0.0605	0.0713	0.0812
	0.30	0.0000	0.0368	0.0521	0.0646	0.0757	0.0858
	0.40	0.0000	0.0445	0.0607	0.0735	0.0846	0.0946
	0.50	0.0000	0.0552	0.0712	0.0834	0.0938	0.1030
	0.60	0.0000	0.0700	0.0842	0.0946	0.1033	0.1109
	0.70	0.0000	0.0907	0.1005	0.1075	0.1132	0.1183
	0.80	0.0000	0.1197	0.1212	0.1225	0.1238	0.1252
Cubic	**0.00**	0.0000	0.0125	0.0158	0.0192	0.0226	0.0261
G3	**0.05**	0.0000	0.0131	0.0172	0.0214	0.0256	0.0297
	0.10	0.0000	0.0138	0.0188	0.0237	0.0285	0.0332
	0.15	0.0000	0.0147	0.0206	0.0261	0.0314	0.0365
	0.20	0.0000	0.0159	0.0225	0.0285	0.0343	0.0398
	0.25	0.0000	0.0173	0.0245	0.0310	0.0371	0.0429
	0.30	0.0000	0.0190	0.0267	0.0336	0.0399	0.0459
	0.40	0.0000	0.0234	0.0318	0.0390	0.0454	0.0515
	0.50	0.0000	0.0295	0.0379	0.0448	0.0509	0.0565
	0.60	0.0000	0.0380	0.0455	0.0513	0.0564	0.0611
	0.70	0.0000	0.0501	0.0549	0.0587	0.0621	0.0652
	0.80	0.0000	0.0673	0.0670	0.0672	0.0679	0.0687

References

1. Boyer, H.E., *Atlas of fatigue curves*. 1985: Asm International.
2. Duerden, F.C. and J.J. Swiss. *KURDISTAN—AN UNUSUAL SPILL SUCCESSFULLY HANDLED*. in *International Oil Spill Conference*. 1981. American Petroleum Institute.
3. Knott, J.F., *Fundamentals of fracture mechanics*. 1973: Gruppo Italiano Frattura.
4. Collins, J., G. Potirniche, and S. Daniewicz, *Failure models: Performance and service requirements for metals.* Mechanical Engineers' Handbook, Volume 1: Materials and Engineering Mechanics, 2015. **1**: p. 703.
5. Suresh, S., *Fatigue of materials*. 1998: Cambridge university press.
6. Marigo, J., *Modelling of brittle and fatigue damage for elastic material by growth of microvoids.* Engineering Fracture Mechanics, 1985. **21**(4): p. 861-874.
7. Sharma, B. and O. Gandhi, *Digraph-based reliability assessment of a tribo-pair.* Industrial Lubrication and Tribology, 2008.
8. Westergaard, H.M., *Bearing Pressures and Cracks.* Journal of Applied Mechanics, 1939. **6**: p. 49–53.
9. Irwin, G.R., *Analysis of Stresses and Strains near the End of a Crack Traversing a Plate.* Journal of Applied Mechanics, 1957. **24**: p. 361–364.
10. Sneddon, I.N., *The Distribution of Stress in the Neighbourhood of a Crack in an Elastic Solid.* Proceedings, Royal Society of London, 1946. **A-187**: p. 229–260.
11. Williams, M.L., *On the Stress Distribution at the Base of a Stationary Crack.* Journal of Applied Mechanics, 1957: p. 109–114.
12. Irwin, G., *Fracture dynamics, Fracturing of Metals. American Society of Metals.* Cleveland, Ohio, 1948: p. 296.
13. Irwin, G., *Handbuch der Physik, vol. 6.* Springer Verlag (Berlin), 1958.
14. Williams, M.L., *On the stress distribution at the base of a stationary crack.* 1957.
15. Sneddon, I.N. and M. Lowengrub, *Crack problems in the classical theory of elasticity.* 1969, 221 P, 1969.
16. Labarrere, C.A., et al., *Early prediction of cardiac allograft vasculopathy and heart transplant failure.* American Journal of Transplantation, 2011. **11**(3): p. 528-535.
17. Rice, J.R., *A path independent integral and the approximate analysis of strain concentration by notches and cracks.* 1968.
18. Cipolla, R.C., *Technical basis for the revised stress intensity factor equation for surface flaws in ASME Section XI Appendix A*. 1995, American Society of Mechanical Engineers, New York, NY (United States).
19. Newman Jr, J. and I. Raju, *Analyses of Surface Cracks in Finite Plates under Tension or Bending Loads (NASA TP-1578).* NASA: Hampton VA, USA, 1979.
20. Saad, D., G. Dundulis, and R. Janulionis, *Numerical simulation of SIF in Es-Salam research reactor vessel.* Engineering Failure Analysis, 2019. **96**: p. 394-408.
21. Saad, D., G. Dundulis, and R. Janulionis, *Calculation of SIFs for semi-elliptical surface cracks in U-shaped bellows expansion joints of Es-Salam research reactor vessel.* Engineering Failure Analysis, 2020. **111**: p. 104481.
22. Oplt, T., et al. *Numerical simulations of semi-elliptical fatigue crack propagation*. in *AIP Conference Proceedings*. 2020. AIP Publishing LLC.